Synthesis of the distribution of subsidence of the lower Ganges-Brahmaputra Delta, Bangladesh

Michael S. Steckler [a,*], Bar Oryan [a,b], Carol A. Wilson [c], Céline Grall [d], Scott L. Nooner [e], Dhiman R. Mondal [f], S. Humayun Akhter [g], Scott DeWolf [h], Steve L. Goodbred [i]

[a] Lamont -Doherty Earth Observatory of Columbia University, Palisades, NY, United States
[b] Department of Earth and Environmental Sciences, Columbia University, Palisades, NY, United States
[c] Department of Geology and Geophysics, Louisiana State University, Baton Rouge, LA, United States
[d] LIENSs, La Rochelle University, La Rochelle, France
[e] Department of Earth and Ocean Sciences, University of North Carolina Wilmington, Wilmington, NC, United States
[f] MIT Haystack Observatory, MIT, Westford, MA, United States
[g] Department of Geology, University of Dhaka, Dhaka, Bangladesh; now Vice Chancellor, Bangladesh Open University, Gazipur, Bangladesh
[h] Department of Environmental Engineering and Earth Sciences, Clemson University, Clemson, SC, United States
[i] Department of Earth and Environmental Sciences, Vanderbilt University, Nashville, TN, United States

ARTICLE INFO

ABSTRACT

Deltas, the low-lying land at river mouths, are sensitive to the delicate balance between sea level rise, land subsidence and sedimentation. Bangladesh and the Ganges-Brahmaputra Delta (GBD) have been highlighted as a region at risk from sea-level rise, but reliable estimates of land subsidence have been limited. While early studies suggested high rates of relative sea-level rise, recent papers estimate more modest rates. Our objective is to better quantify the magnitude, spatial variability, and depth variation of sediment compaction and land subsidence in the lower GBD to better evaluate the processes controlling them and the pattern of relative sea level rise in this vulnerable region. We combine subsidence and compaction estimates from hand-drilled tube wells and historic sites (1–5 mm/y), GNSS and river gauges (4–8 mm/y) and RSET-MH and borehole vertical strainmeters (9–10 mm/y) in SW Bangladesh. The differences between the different types of measurements reflect the different timescales, spatial distribution and depth sensitivity of the different observations. Rates are lower for times >300y providing data on the timescale of compaction. We also observe differences related to the degree to which different devices measure shallow and deep subsidence. Higher values reflect a greater component of subsidence from young shallow deposits from soil compaction and organic matter degradation. Thus, we observe different rates for different environments and physical settings. These differences indicate that in planning adaptation for rising sea level, hard construction with a solid foundation may experience different subsidence rates than open fields or reclaimed land with recent natural or anthropogenic sedimentation.

Significance statement: Land subsidence increases the impact of sea level rise. We combine six different types of measurements that examine land subsidence in coastal Bangladesh. The results show that causes of subsidence, including compaction of the sediments varies both spatially and with depth, and that compaction and organic matter degradation from young shallow deposits is a significant contribution to subsidence. This suggests that hard construction with a solid foundation, such as buildings and embankments, may experience a lower subsidence rates than open fields or reclaimed land with recent natural or anthropogenic sedimentation.

1. Introduction

Deltas, the low-lying land at river mouths, are particularly sensitive to the delicate balance between sea level rise, land subsidence and sedimentation (Milliman et al., 1989). An estimated 350 million people globally inhabit these vulnerable landscapes (Edmonds et al., 2020), thus processes that control growth versus loss of land is vital to the stability of coupled human-natural deltaic systems (Syvitski et al., 2009;

* Corresponding author.
  E-mail address: steckler@LDEO.columbia.edu (M.S. Steckler).

Tessler et al., 2015). Low-lying river deltaplains grow by receiving sediments transported to the coast. On the other hand, the weight of the sediments causes compaction and isostatic loading that induces subsidence, which reduces the growth of the delta. Human modification, especially subsurface fluid withdrawal, can further exacerbate subsidence (e.g., Dixon et al., 2006; Akhter et al., 2009; Minderhoud et al., 2017; Erkens et al., 2016). Upstream damming and river diversions have substantially decreased the sediment supply to many deltas (e.g., Syvitski et al., 2005; Blum and Roberts, 2009; Giosan et al., 2014; Kondolf et al., 2014; Gebremichael et al., 2018). A detailed understanding of the balance between sea level rise, sedimentation and subsidence is critically important for assessing the sustainability of deltas. The elevation balance at deltas can be summarized by the following equation modified from Syvitski et al. (2009):

$$\Delta_{REL=} -\Delta E - C_n - C_a - M + A \tag{1}$$

where Δ_{REL} is the rate of relative vertical change in delta surface elevation, ΔE is Eustatic sea level rise rate, C_n is the rate of subsidence from Natural Compaction, C_a is the subsidence rate of Accelerated Compaction due to human activities, M is the rate of vertical crustal Movement (including both tectonics and isostatic motions), and A is the sediment Aggradation rate. Thus, multiple components of subsidence increase elevation loss while sedimentation counters elevation loss by the deposition of organic and inorganic material in areas of new accommodation.

As the boundary between land and sea, a number of studies have found that deltas are at risk from sea level rise and climate change, and are becoming increasingly vulnerable to flooding, erosion, and salinization (Ericson et al., 2006; Syvitski et al., 2009; Ostanciaux et al., 2012; Tessler et al., 2015, 2018). A recent study (Nienhuis et al., 2020) found globally deltas are still gaining land, but with accelerating sea level rise and anthropogenic changes this is likely not sustainable. However, most large and medium size deltas have insufficient sediment supply to maintain their current size (Giosan et al., 2014) and there is declining sediment supply to most major deltas due to climate change and human intervention (Dunn et al., 2019). While accurate estimations of ΔREL are critically needed for addressing the human sustainability in deltas, these estimates are plagued with difficulties, such as constraining all the parameters that play out both locally and regionally, and having sufficient long-term instrumental records that capture interannual variability. In order to fully understand ΔREL, a variety of measurements are required, as different instruments provide distinct information on compaction and subsidence. For example, different instrument anchoring depths yields different results (Keogh and Törnqvist, 2019). This can lead to a large variability in measurements, such that the regional pattern is difficult to distinguish. This is the case for the Ganges-Brahmaputra Delta (GBD), the largest delta in the world (Brown and Nicholls, 2015; Paszkowski et al., 2021). We present here a coherent synthesis of vertical elevation change, compaction, and subsidence in this region, revisit previously
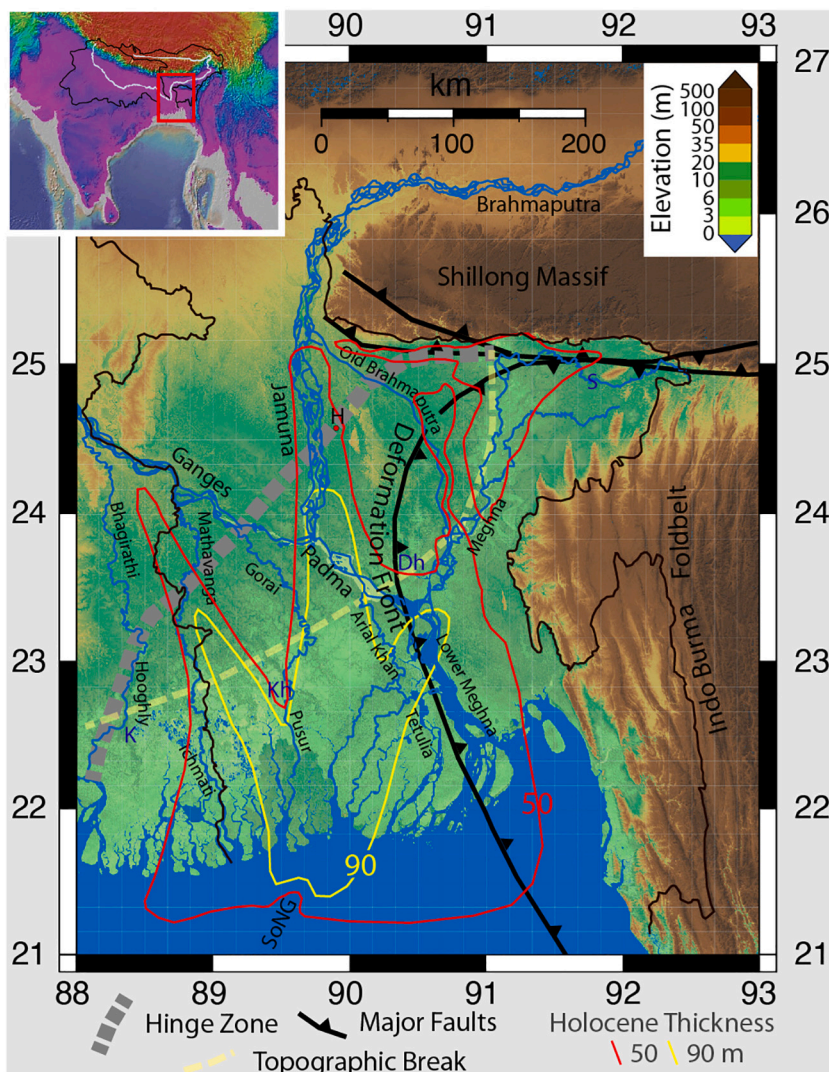

Fig. 1. Location map of Bangladesh and the Ganges-Brahmaputra Delta showing major tectonic and sedimentary boundaries, and significant rivers. The Hinge Zone is the transition between the Indian craton and the Bengal Basin with up to 20 km of sediments. The Topographic Break is the boundary between the Fluvial Fan Delta to the north and the flatter Fluvial-Tidal Delta to the south (Wilson and Goodbred, 2015). K = Kolkata, Kh = Khulna, Dh = Dhaka, S = Sylhet, H = Hazipur-1 well, SoNG = Swatch of No Ground Canyon. The inset shows the regional topography with the outline of the drainage basin of the Granges, Brahmaputra and Meghna River basins outlined in black and the rivers in white. The red box shows the location of the detailed figure. (For interpretation of the references to colour in this figure legend, the reader is referred to the web version of this article.)

published data, and update this dataset with newly acquired data. Finally, we analyze these datasets together to extract significant information about the temporal and spatial variability of subsidence in the GBD, one of the most densely populated regions of the world.

2. Regional setting

The GBD, the largest delta in the world, is formed by two of the world's major rivers (Fig. 1). The GBD has been highlighted as a region at risk from rising river and ocean water levels (e.g., Milliman et al., 1989; Ericson et al., 2006; Syvitski et al., 2009; Tessler et al., 2018). It receives >¾ of the water and sediment drained from the Himalayas (Milliman and Farnsworth, 2011) creating a fertile and densely-populated delta in which >130 million people live. This low-lying land, with half of Bangladesh at elevations <10 m, undergoes riverine flooding every monsoon season: in a normal year, 20–25% of the land is submerged, but can reach 60–70% during an extreme flood (Mirza, 2003). The GBD is still net gaining land, with growth at the river mouth outpacing land loss along the coast farther west (e.g., Allison, 1998; Brammer, 2014). While parts of the delta near the Lower Meghna River mouth (Fig. 1) are receiving sufficient sediment and gaining land, other regions away from the major rivers are in decline (Wilson and Goodbred, 2015). In the tidal delta near the coast, sediment supply averages 11 mm/y in the Sundarbans (Rogers et al., 2013) and 23 mm/y farther east (Rogers and Overeem, 2017) with large variability. Anthropogenic channel infilling in the delta interior also contributes to net land gain (Wilson et al., 2017). However, large tracts of coastal Bangladesh have been embanked (poldered), halting sediment delivery within the polders. This region, where natural and anthropogenically-enhanced subsidence is no longer offset by sedimentation, is where the land is at greatest risk (Wilson and Goodbred, 2015; Auerbach et al., 2015). This has exacerbated waterlogging of the embanked islands and a shift from rice cultivation to shrimp farming (Alauddin and Hamid, 1999).

In the fluvial delta farther upstream, sedimentation is focused near the rivers while subsidence is distributed broadly. Elevation increases near rivers while areas farther away subside. This increasing elevation contrast through time drives river avulsions (Slingerland and Smith, 2004), thereby spreading the sediments delta-wide over sufficiently long (geologic) timescales (Reitz et al., 2015). Major tributaries to the upper delta, such as the Tista are also highly avulsive, in part associated with flexural loading across the hinge zone (Grimaud et al., 2020). The result is a dynamic landscape where sedimentation and subsidence patterns are continually in flux. Around the turn of the 19th century, there was the well-known westward avulsion of the Old Brahmaputra River to its present Jamuna channel (Fig. 1). This is one of several Holocene avulsions of the Brahmaputra, which averages avulsions every ~1800y (Reitz et al., 2015; Sincavage et al., 2017). The Ganges has also undergone avulsions. Prior to the mid 1600s, the Hooghly River (Fig. 1) was the main channel of the Ganges River (Eaton, 1993; Parua, 2010). The Mathabhanga, Gorai, Arial Khan, among others, were major distributaries to the east of the Hooghly. The shift of the Ganges to the Padma led to a reduction of water and sediment to these channels. The resulting increased salinity incursion in the lower deltaplain led to the building of polders (embankments) in the 1960s and 70s to improve agricultural production. Now, the Farakka Barrage in India diverts water from the Ganges into the Hooghly and efforts have been made in Bangladesh to restore flow to the Gorai. Sometime in the late 19th century the Ganges shifted from flowing down the Arial Khan and Tetulia channels to join the Brahmaputra in the Lower Meghna channel (Fig. 1). As a result, the Lower Meghna is widening while the Arial Khan and Tetulia are narrowing (Allison, 1998; Brammer, 2014).

The interplay of sedimentation, subsidence and sea level at the GBD is further complicated by active tectonics at the eastern half of the delta (Fig. 2). The IndoBurma subduction zone (IBSZ) is the along strike continuation of the Sumatra subduction zone. While most subduction zones are submarine, in Bangladesh the incoming plate is capped by the
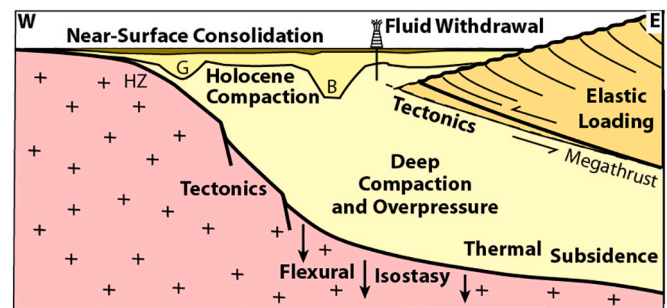

Fig. 2. Cartoon illustrating subsidence processes active in the Ganges-Brahmaputra Delta in a schematic, not to scale, cross section. In the eastern delta, the tectonics of the IndoBurma foldbelt and Shillong Plateau are significant. Elastic loading from the earthquake cycle adds interseismic subsidence that is reversed during earthquakes. Both the tectonics and sedimentation contribute to flexural isostatic loading of the lithosphere. The old passive margin of seaward of the Hinge Zone (HZ) is subject to thermal subsidence, but the rate is very low for this older margin. Within the sediments, deep compaction over kilometer-scale depth contributes, but is limited where overpressure slows fluid expulsion. More of the sediment compaction occurs in the Holocene sediments that have filled the incision from the last glacial period (G and B mark the Ganges and Brahmaputra incised valleys). In the very near surface, additional processes, such as organic matter degradation, come into play and contribute to large amount of compaction in the upper few meters of sediments.

GBD with its 16–20 km of sediment (Singh et al., 2016; Mitra et al., 2018; Ismaiel et al., 2019) and as a result, the accretionary prism is entirely subaerial (Fig. 1). It encompasses to a > 300 km area hosting a series of divergent anticlines (Betka et al., 2018). The less well-developed frontal anticlines are blind and buried by the delta, but are known from gas exploration. The position of the deformation front (Fig. 1) is based on mapping these anticlines (Betka et al., 2018). East of the deformation front, there is additional subsidence from flexural loading, and uplift from shortening and thickening in the accretionary prism. Furthermore, the earthquake cycle produces cycles of subsidence and uplift through elastic loading of the megathrust underlying the entire area (Fig. 2). Akhter (2010) suggested that the avulsion of the Old Brahmaputra to the current Jamuna channel (Fig. 1) may have been due to tectonics, perhaps triggered by a 1787 earthquake. Furthermore, earthquakes can produce pulses of sediment delivery downstream. Enhanced sediment flux from the 1950 Assam earthquake has been documented (Goswami, 1985; Sarma, 2005; Sarker and Thorne, 2006) along with progressive changes in the Brahmaputra River width and braiding from the sediment pulse. Given these additional complexities, this paper's primary focus is on the components of elevation change, compaction, and subsidence in the non-tectonic part (i.e., west of deformation front, Fig. 1) of the GBD in southwest Bangladesh as defined by Grall et al. (2018).

The extensive natural and anthropogenic changes in the sediment distribution within the GBD illuminate the importance of addressing of how subsidence is distributed across the delta, particularly on the lower tidal deltaplain. While sedimentation drives compaction and isostatic adjustment, the long timescales of these responses mean that they have significant lags and that subsidence continues after rivers have shifted their depocenters. This sets up a cycle of delta lobe progradation followed by degradation after abandonment, similar to the Mississippi Delta (Allison et al., 2003). However, reliable estimates of land subsidence and relative sea level rise (the combination of sea level rise and subsidence) at the GBD have been limited. Early global studies that included the GBD suggested high rates of relative sea level rise (Ericson et al., 2006; Syvitski et al., 2009; Tessler et al., 2018), while more recent local papers suggest modest rates (Pethick and Orford, 2013; Grall et al., 2018; Becker et al., 2020). Knowing the current rates of sediment compaction, tectonic land movement and isostatic loading (Fig. 2) is

critical for understanding the sedimentation patterns in the GBD and the prospect for near future land loss and salinization. Recent studies (Karpytchev et al., 2018; Krien et al., 2019), suggest that isostatic loading by the sediments contribute significantly to the subsidence of the delta. The contribution of sediment compaction and organic matter degradation may be large at the GBD (Higgins et al., 2014) given the high sedimentation rates (Rogers et al., 2013, Rogers and Overeem, 2017) and thicknesses (Singh et al., 2016; Mitra et al., 2018; Ismaiel et al., 2019). While the GBD is predominantly considered a mineralogenic deltaplain, some organogenic wetland areas exist, and Higgins et al. (2014) documented that these fine-grained organic regions have experienced substantial subsidence after reclamation. In addition, groundwater extraction is significant near Dhaka (Akhter et al., 2009), but widespread irrigation is broadly lowering the water table (Shamsudduha et al., 2009).

Quantitative estimates of these multiple factors throughout the GBD are poorly known. Chamberlain et al. (2020) provided an overview of methods for quantifying the sedimentation and subsidence history of the GBD, and a summary of efforts to date. Here we compile previous and recently published subsidence measurements with new evaluations of GNSS, tide gauge, and historical building measurements, and discuss the nuances between shallow vs deep and short- vs long-term processes. Our objective is to better quantify the magnitude, spatial variability, and depth variation of compaction and subsidence in the GBD to better evaluate the processes controlling it and the pattern of relative sea level rise in this vulnerable region.

3. Compaction processes

As sediments are buried, they undergo a variety of sediment compaction and consolidation processes resulting in the loss of porosity and decrease in sediment layer thicknesses through time and with depth, inducing subsidence of the overlying strata (Fig. 2). With greater depth, sediment grains reorganize into more compact arrangements, particularly platy clay minerals that rotate to horizontal orientations. Smaller grains can fill pores between larger grains. With increasing pressure and temperature, grains can dissolve at inter-grain contacts and reprecipitate into pore spaces to further lower porosity. Additional dissolved minerals may be transported through the basin and contribute to cementation. Chemical reactions, such as dehydration of clays, further reduce the sediment water content. At still greater depth, metamorphic reactions reduce sediment volume. The progressive reduction of porosity with depth or lithostatic overburden has been modeled by a variety of empirical formulas, often with an exponential form (e.g., Athy, 1930; Terzaghi and Peck, 1967; Sclater and Christie, 1980; Gluyas and Cade, 1997; Kooi and DeVries, 1998; Bahr et al., 2001; Sheldon and Retallack, 2001; Kominz et al., 2011). The initial porosity of the sediments and its decay with depth depend strongly on the lithology of the sediments. Organic-rich clay and silt generally have higher initial porosities and undergo greater compaction than coarser sediments (Sheldon and Retallack, 2001; Meckel et al., 2007; van Asselen, 2011; Kominz et al., 2011). Another factor is that low permeability sediments, such as shale, may hinder the upward flow of fluids, slowing or halting compaction and creating overpressure in the sediments (e.g., Gluyas and Cade, 1997; Gordon and Flemings, 1998). In the GBD, extensive overpressure is present below depths of 3–5 km where sediments are mainly deeper-water shales (Zahid and Uddin, 2005).

Another important consideration impacting compaction is the incision of the delta during the last glacial maximum (LGM). While lowstand deltas are found offshore near the shelf edge (Palamenghi, 2012), within the GBD, a large valley 60-90 m deep was incised into older Pleistocene-aged sediments during the LGM (Fig. 1, Pickering et al., 2014; Goodbred et al., 2014). Previously buried sediments do not significantly decompact with unloading (Chapman, 1983). Further compaction only occurs when the valleys are subsequently filled and overburden pressure exceeds the previously level. Thus, during the Holocene, compaction in the GBD has primarily occurred in the Holocene-aged sediments and not in the underlying older strata (Fig. 2).

At shallow depths, compaction of young sediments can be rapid, particularly for highly porous muddy sediments (Hedberg, 1936; Kominz et al., 2011; van Asselen, 2011). Peat and other organic rich soils undergo even more rapid compaction in the near surface than other soils (Sheldon and Retallack, 2001; van Asselen, 2011). Oxidation of peats due to groundwater lowering can cause significant subsidence (van Asselen et al., 2018). However, few true peats with very high percentages of organic matter are found in the GBD (Brammer, 1990; Goodbred et al., 2003, Best et al. 2007). Large water level fluctuations and biologic respiration lead to oxidation of most organic material before it is deeply buried. In addition, roots occupy soil volume, which can reach 10–20% in the Sundarbans mangrove forest in the near surface (Auerbach et al., 2015) leading to thickness loss as the plants senesce, dewater, and are oxidized with burial. Bioturbation and animal burrows can further increase the porosity at very shallow levels. These effects can contribute to a large amount of effective sediment compaction in the upper few meters of the sediment column.

4. Previous estimates of subsidence in the GBD

A limited number of studies have examined subsidence rates in the GBD. Alam (1996) and Hoque and Alam (1997) compiled radiocarbon dates on Holocene samples and obtained subsidence rates from 0.53 (Kolkata) to 5.48 mm/y (Khulna) (Fig. 1), but suggested that rates could reach 20–30 mm/y in places. Alam (1996) assigned the reported top of the Plio-Pleistocene Dupi Tila formation in the 1960 Hazipur-1 well as corresponding to the beginning of the Holocene. As a result, he estimated a subsidence rate of 22 mm/y that is likely too high (see supplement). This was used in a global analysis of delta subsidence (Ericson et al., 2006) to suggest a high subsidence rate in the GBD. Radiocarbon data on auger and vibracores up to 7 m depth across the lower delta plain (Allison et al., 2003) indicated sediment accumulation rates of 1–7 mm/y and subsidence rates of 1–4 mm/y. A summary of the papers discussed in this section is provided in Table S1.

In a study of global deltas, Syvitski et al. (2009) suggested a GBD subsidence rate of up to 18 mm/y. Their estimate is based on a high rate of subsidence at the Khepupara tide gauge. However, our examination of the 1977–2010 record of this gauge using hourly Bangladesh Inland Water Transportation Authority (BIWTA) data shows several decadal-scale changes in rates (Fig. 3), with at least one change in 2000 corresponding to when the gauge was relocated based on local interviews. The publicly available data (1987–2000) from the Permanent Service for Mean Sea Level (PSMSL) corresponds closely to the period of high subsidence of the gauge, and thus should be regarded as an overestimate (Fig .3). Ostanciaux et al. (2012) studied global trends of coastal vertical motion and estimated high rates at the GBD of 11–20 mm/y, again biased by the public Khepupara gauge data.

In contrast, Sarker et al. (2012) examined plinth elevations relative to the surrounding ground levels (Fig. 6) at four historic sites that are 200–600 years old and determined low subsidence rates of 0–2.5 mm/yr. However, as described below, a reanalysis of one site, the Shakher Temple in the Sundarbans, yields a higher rate of 3.4 mm/y (Chamberlain et al., 2020). At Katka Beach in the Sundarbans, Hanebuth et al. (2013) discovered 300-year old salt kilns uncovered by coastal erosion. The kilns would have been built just above spring high tide level indicating 4.1 mm/y subsidence. The remains of additional salt kiln sites in the region have been discovered and are being dated (H. Kudrass, Pers. Comm., 2020).

Brown and Nicholls (2015) compiled a comprehensive suite of >200 measurements of subsidence in the GBD. Methodologies included carbon dating, borings/wells/auger logs, archaeological sites, InSAR, GNSS, optically stimulated luminescence dating, geomorphology, estimates of compaction from groundwater depletion, and magnetostratigraphic dating. However, by mixing multiple types of measurements
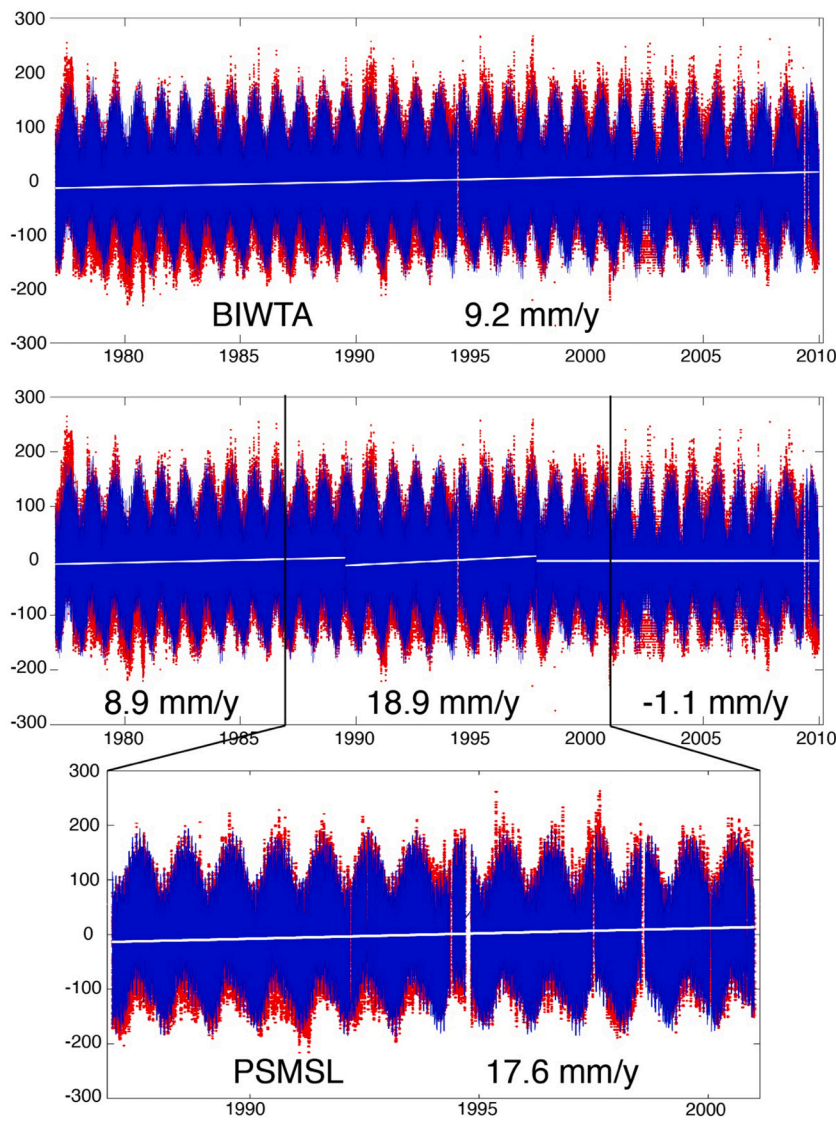
Fig. 3. Water level data from the Khepupara tide gauge. The top shows hourly data from the Bangladesh Inland Water Transportation Authority (BIWTA) in red and a tidal model from t_tide (Pawlowicz et al., 2002) in blue showing a mean sea level rise rate of 9.2 mm/y, indicated by a white line. However, examination of the data shows variable rates of sea level rise. The middle shows fits to the three distinct regimes with the rates noted below each segment. The bottom shows the more limited publicly-available time series from PSMSL. It corresponds approximately to the central portion of the longer times series when the apparent sea level rise rate was greatest. (For interpretation of the references to colour in this figure legend, the reader is referred to the web version of this article.)

with insufficient constraints on their settings, they obtained subsidence rates that varied from 44 to −1 mm/y, including broad ranges of values at individual sites. Their comprehensive mixture of samples with limited context also shows the "Sadler effect" (Sadler, 1981), with mean subsidence rates decreasing with increasing timescale of measurement. A critical problem is the need to distinguish between subsidence and sediment accumulation rates. For example, if incision by a river is followed by rapid deposition when the river migrates or avulses, the net effect is younger river channel sediments replaces older sediments. This "channel incision effect" yields incorrect high apparent subsidence rates (Fig. 4). Grall et al. (2018) used >400 tube wells with almost 200 ^{14}C dates (Fig. 5), as well as seismic data along the Brahmaputra River and
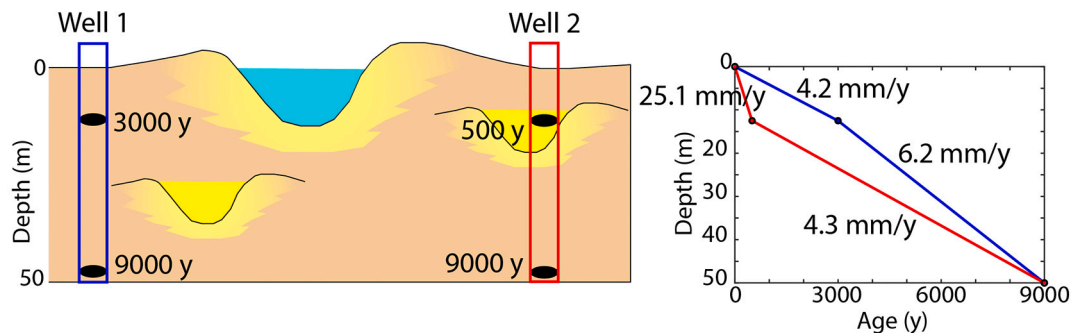

Fig. 4. Cartoon and plot illustrating the channel incision effect. Well 1 records a continuous section with close to linear subsidence rates based on two dated samples. In Well 2, a river channel incised into the section, depositing sandy sediments before avulsing to a newer position. The dates from this well record an anomalously high apparent subsidence rate due to the younger river deposits and an underestimated subsidence rate for the lower section, illustrating the need for the context of dated samples.
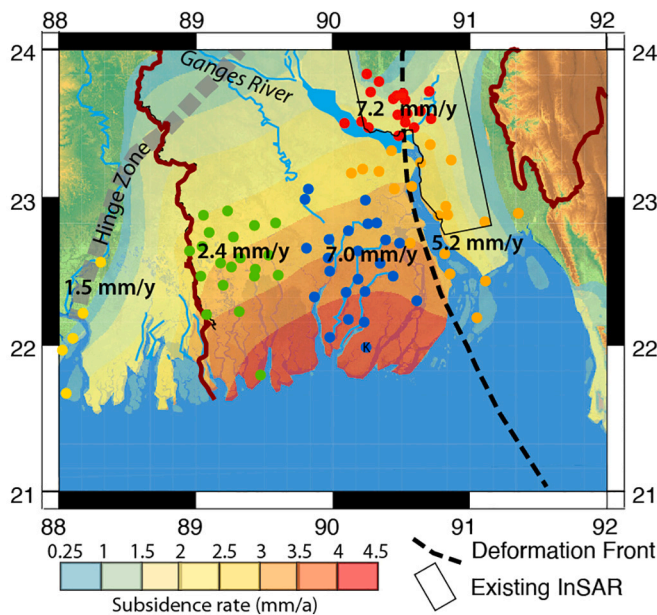
Fig. 5. Map showing contours of Holocene average subsidence rates in the GBD (41). Subsidence increases seaward from the Hinge Zone. Superimposed are the locations of the river gauges (Becker et al., 2020) as colored dots with the corresponding average rates on subsidence over a 20-year period for each set. The K indicates the position of the tide gauge at Khepupara.

offshore, to estimate average Holocene subsidence rates. The authors identified and removed samples affected by the channel incision effect, and distinguished components due to sediment accumulation, eustatic sea level rise and subsidence. Results revealed a systematic variation of subsidence rates across the delta. In the lower GBD, subsidence increases from near zero rates landward of the Hinge Zone to 4.5 mm/yr at the southern coast of Bhola Island (Fig. 5). The Hinge Zone is the track of the Eocene shelf edge, which also corresponds to the boundary between the thinly sediment-covered Indian craton and the thick sedimentary depocenter of the Bengal Basin (Fig. 1; Steckler et al., 2008).

Recently, Becker et al. (2020) analyzed groups of river and tide gauges to reconstruct subsidence rates in the delta (Fig. 5). The averaging of 19–24 stations for each zone, along with the corrections and analysis in the paper, minimized the effect of poor tide gauges, such as Khepupara. They estimate a maximum of up to 7 mm/y subsidence for the period of 1993–2012. This is noticeably higher than the Holocene rates of Grall et al. (2018) (Fig. 5), but the pattern is generally coherent for the different morphodynamic units (Grall et al., 2018). In the tectonic areas east of the IBSZ deformation front, elastic loading by the locked megathrust (Steckler et al., 2016) is expected to contribute 3–4 mm/y of subsidence (Oryan et al., 2020) that would be countered by earthquake related uplift in the average Holocene rates, which are significantly lower.

GNSS geodesy provides another means of assessing current subsidence rates. Our GNSS stations in Dhaka and Sylhet showed locally high subsidence rates of 12 mm/y (Fig. 1, Steckler et al., 2010). Reitz et al. (2015) expanded the results to include 18 stations. Sites in NW Bangladesh at or landward of the Hinge Zone showed subsidence rates <1 mm/y, while sites in Sylhet, a tectonically active basin, showed high rates (7–12 mm/y). The high subsidence rate in Dhaka at 12 mm/y from groundwater withdrawal was confirmed in the longer time series. Rates in the foldbelt farther east were variable depending on the structural position of the GPS site. Their three sites in the coastal belt showed moderate but variable rates of 3–8 mm/yr.

Higgins et al. (2014) used InSAR measurements with the ALOS-1 satellite to create a map of subsidence rates across a > 10,000 km^2 swath of central Bangladesh (location in Fig. 5). They obtained rates

from 0 to >18 mm/yr, with the lowest rates primarily in Pleistocene Madhupur Clay and the highest rates in Holocene organic-rich muds. One high subsidence area follows an eastern branch of the Lower Meghna that previously flowed past Noakhali (approximately the position of the M in Lower Meghna in Fig. 1), but was filled with sediments following the 1950 Assam earthquake (Sarker et al., 2013). These young deposits are clearly undergoing rapid compaction. Dhaka has high rates of subsidence from groundwater withdrawal (Steckler et al., 2010), and the InSAR (Higgins et al., 2014) shows variable rates that correlate with the underlying geology. Further investigations using InSAR from the Sentinel-1 satellite are ongoing (Woods et al., 2019).

5. Updated subsidence rates

We present our efforts to expand and improve the data on subsidence of the GBD and attempt to construct a coherent pattern of subsidence taking into account the different timescales of the measurements, the spatial distribution of sites in the context of the geology of the delta, and the depth component of each type of measurement. This synthesis has been supported by the Bangladesh Water Development Board contract CEIP-1/C3/C4 building on earlier U.S. government grants.

5.1. Revised long-term Subsidence from Historic Sites

As mentioned above, human historic sites can provide evidence of subsidence over hundreds of years. Sarker et al. (2012) examined four historic sites, two Hindu temples and two Muslim mosques. A key component in determining subsidence from historic sites is identifying the plinth level, the base or platform upon which the building is built (Fig. 6). Construction typically includes a base that is built up from the original Tidal Platform Level (TPL) to the Homestead Platform Level (HPL), which is close to SHWL (Spring High Water Level), and then a plinth level (Fig. 6) that is 0.5–0.8 m higher to protect against floods. The thickness of the homestead platform is equal to a/2 (Fig. 6), or half the difference between the NHWL (Neap High Water Level) and SHWL, placing the TPL at mean high water.

For the two 15th century mosques at Bagherat, subsidence is estimated as 1.9 ± 0.6 mm/y (Sarker et al., 2012). Lower rates of 1.25 mm/y and 0.14 ± 0.74 mm/y were found for the two ancient Hindu temples, the Shakher Temple and Doyamayee Mondir. We re-evaluated the subsidence at one of these temples during a visit (Fig. 7). We believe that the plinth level of the 400-year old the Shakher Temple in the Sundarbans was misidentified. In their analysis of the temple, Sarker et al. (2012) placed the plinth level at the entrance of the temple at the top of the stairs, even with the interior of the temple (Fig. 7). While Muslim mosques are communal prayer halls that often are open at ground level, Hindu temples are commonly raised, as they are the home to gods (in this case, the Goddess Kali). Thus, one ascends the temple to enter the home of the goddess (Sharma and Deshpande, 2017). We believe the previous evaluation (Sarker et al., 2012) missed this architectural feature. Instead, we located a ridge in the bricks near ground level (Fig. 7) that we associate with the plinth level (Chamberlain et al., 2020). In addition, augering discovered a buried brick layer 1.5 m below the surface. We interpret the brick layer as the original TPL level minus any excavation for preparing and leveling the site for construction. The brick layer and revised plinth level are consistent and yield a new subsidence rate of 3.4 ± 0.5 mm/y (details in the supplement). We have not visited the other Hindu Temple, but it may have the same issue, so we exclude it from our calculations.

5.2. New recent shallow subsidence from RSET-MH

Rod surface elevation tables and marker horizons (RSET-MH) is a method of determining surface elevation changes and sedimentation rates in deltas and wetlands (Cahoon et al., 1995, 2002). Elevation measurements are made from a rod driven into the ground to the depth
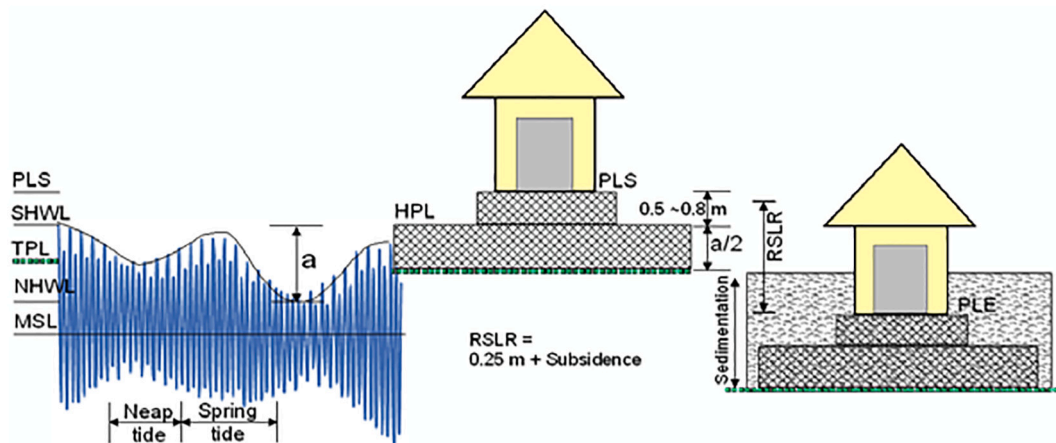
Fig. 6. Diagram (Sarker et al., 2012) illustrating the computation of subsidence for historic sites. RSLR = relative sea level rise with 0.25 m equal to eustatic sea level rise over the period since the historic sites were built; MSL = mean sea level; HPL is the homestead platform level. PLS and PLE are starting and ending plinth level, respectively. See text for other notations.

Fig. 7. Photo of the ~400 year old Shakher Temple in the Sundarbans with a closeup of our interpreted plinth level in the lower left.

of refusal or a maximum 24.38 m (80 ft.) (D. Cahoon, pers. comm., 2009). Following the procedures in Cahoon et al. (2002), a horizontal arm is attached to the rod from which 9 measurements of surface elevation surrounding the site are taken at 8 different positions for a total of 72 measurements. Tile marker horizons are used to measure sediment accumulation rates at each site visit. Shallow subsidence above the base of the rods is determined by the difference between the elevation change and the sedimentation rate. What distinguishes these measurements from those described earlier is that the RSET-MH measure subsidence up to the surface in places with active sediment deposition. Thus, these rates include very shallow and seasonal near surface sediment consolidation and organic matter decomposition. Wilson et al. (2021) has established a network of 22 RSET-MH in the tidal deltaplain of the GBD (Fig. 8) with measurements made twice a year, before and after the monsoon that is responsible for most of the sedimentation. At

Polder 32, there are 8 RSET-MHs, including 4 inside the polder and 4 in the adjoining Sundarbans forest (Bomer et al., 2020). The remaining sites have a pair of RSET-MHs. This enables us to obtain measurements both inside and outside of the embankments around the deltaic islands (polders, $N = 14$), and within the Sundarbans mangrove forest near stream banks and interiors ($N = 8$). Most were installed in 2019 co-located with our GNSS stations to distinguish shallow and deep subsidence (Keogh and Törnqvist, 2019; Karegar et al., 2020). Reliable rates for the new sites are not yet available as approximately 5 years are needed to establish long-term rates for all the measurements (elevation change, sediment accretion, shallow subsidence) and to separate the long-term trends from seasonal variations. Furthermore, our measurements have been disrupted due to the COVID-19 pandemic. However, preliminary results show seasonal shallow subsidence appears to be exacerbated during the dry season, especially in embanked settings
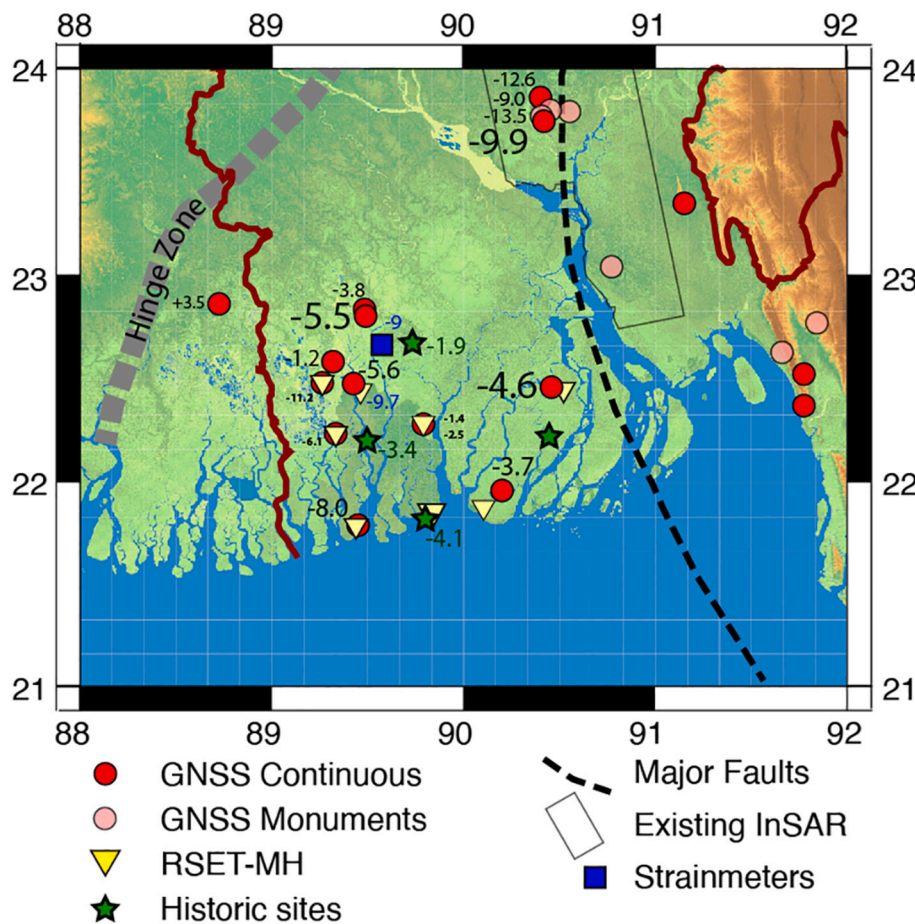
Fig. 8. Subsidence rates in the lower GBD west of the deformation front. Except for historic sites, text size is proportional to the square root of the time series length to represent the reliability of the values. High rates around Dhaka reflect subsidence from ground water withdrawal. Historic sites yield values similar to Holocene average rates in Fig. 4 (Grall et al., 2018). GNSS rates are similar to slightly higher, especially farther west. The vertical borehole strain meter (DeWolf et al., 2017, in prep.) and published RSET-MH value (Bomer et al., 2020) record compaction up to the surface and yield significantly higher rates.

where farmers drain their rice paddies and allow fields to go fallow (Wilson et al., 2021; Bomer et al., 2020). With maturation of the paired RSETs inside and outside of embankments, we should be able to remove this seasonal anthropogenic signal over time. A set of 4 stations in the natural Sundarbans mangrove forest adjacent to Polder 32 established in 2014 yielded seasonal shallow subsidence rates of 7–18 mm/y over a 5-year period, averaging 9.7 ± 1.6 mm/y (Bomer et al., 2020), significantly higher than other measurements despite not including deep subsidence from below the base of the RSET.

5.3. New recent compaction from vertical strainmeters

DeWolf et al. (2017, in prep.) installed two sets of optical fiber strainmeters in hand-drilled wells in Bangladesh. The site in southwest Bangladesh at Bhanderkote, Khulna (called the Khulna compaction meter or KHLC, Fig. 8) contains 6 wells drilled to depths of 20, 40, 60, 80, 100 and 300 m. Each well contains two pairs of optical fibers grouted into the bottom of the well and attached to a concrete monument at the top. The length of each fiber was measured weekly from 2011 to 2016 by local collaborators. In March 2015, the river adjacent to the site was dredged to improve navigation. Readjustment of the river profile led to bank erosion that destroyed KHLC in 2016. Measurements show a seasonal extension of the fibers during the summer monsoon due to clay swelling or poroelasticity with a longer-term subsidence trend. Shortening rates of the fibers generally increase with depth (Fig. 9A) and are consistent with an exponential curve for a total compaction rate of ~9 mm/y for the upper 300 m, with most compaction occurring in Holocene strata above 60 m depth and no compaction below 100 m, within errors. Based on nearby tube well transects, the thickness of the Holocene strata here exceeds 90 m (Figs. 1, 8). Thus, KHLC is located in the broad incised

valley excavated by the Brahmaputra River during the last glacial maximum (Fig. 1). The lack of compaction beneath the Holocene is not unexpected, as the sediments below experienced compaction prior to the lowstand incision.

Additional interpretation needs to take into account recent sedimentation on the site. The river at KHLC was previously >300 m wide (Fig. 9B), but historical imagery shows it narrowed dramatically between 1989 and 1999 (Wilson et al., 2017) and OSL dating of samples from an auger hole at the site shows 4.44 m of deposition since 1987 ± 3 CE due to the channel filling (Chamberlain et al., 2017, 2020). KHLC was installed on the bank of this narrow (<10 m) river in 2011. Boat traffic on the river could only move at high tide leading to the government decision to dredge it. The compaction meter on the river bank was the site of sediment deposition, averaging 10–15 mm/y of tidalites per year until the river was widened (Fig. 9C; Chamberlain et al., 2017, 2020). Deposition likely occurred only during high tides during the monsoon when the river level was sufficient to flood the site. Thus, the high subsidence rate measured in the shallower strainmeters is associated with active sediment deposition and consolidation of recently deposited sediments near the surface.

5.4. New recent subsidence from GNSS

GNSS enables observations using fixed antennas over years to estimate rates of tectonic deformation as well as subsidence or uplift on the order of ±1 mm/y or better. Generally, it takes >2.5 years to determine reliable horizontal rates and >4.5 years for vertical rates (Blewitt and Lavallée, 2002). We find the vertical rates for the DHAK station, with seasonal corrections, stabilized after 6 years. In the GBD, GNSS show a large seasonal component of up to 5–6 mm/y (Steckler et al., 2010). This
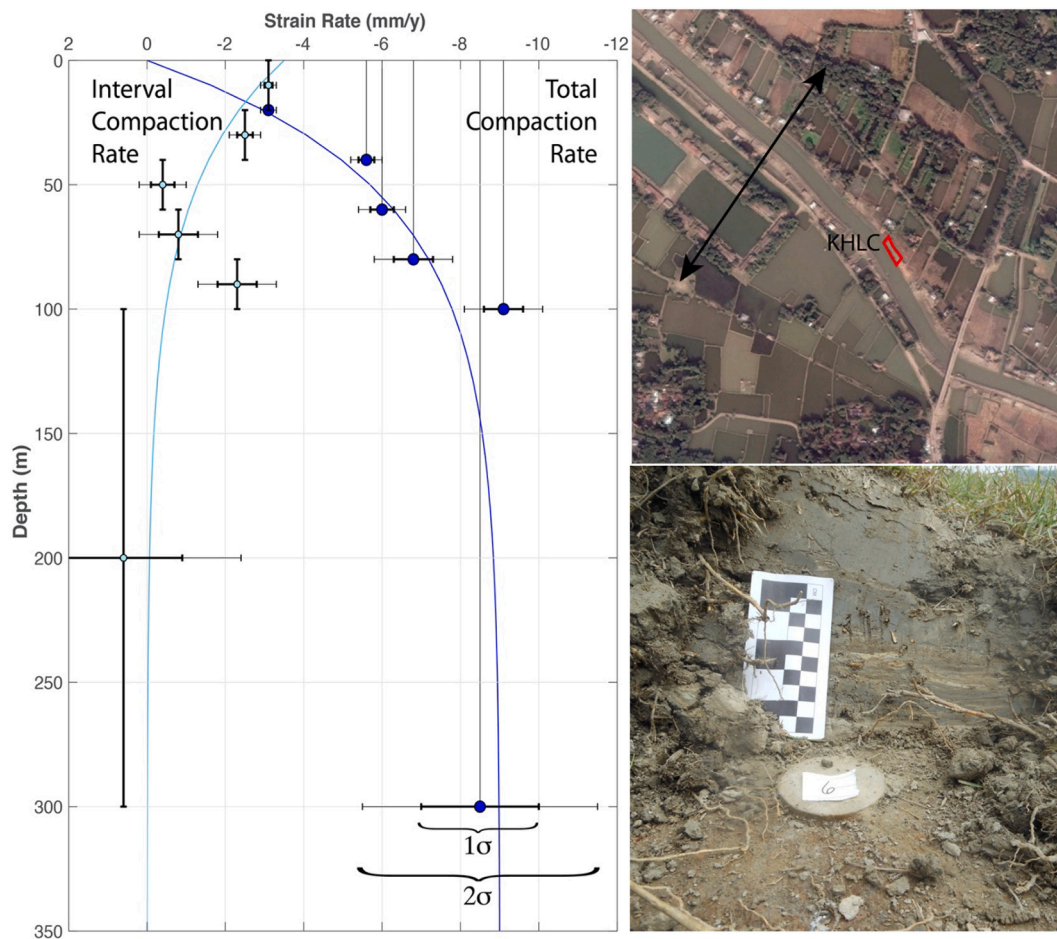
Fig. 9. Results from the KHLC compaction meter. A) plot showing the decrease in compaction with depth. The blue dots show the shortening rate of the different length fibers and teal dots show the differential rate between pairs of fibers. Approximate exponential curves to the data for the total compaction and its derivative are shown. B) Google Earth image of the KHLC site. The wells were installed on the river bank in the red box. The double arrow shows the width of the river before 1989. Notice the large concrete bridge SE of KHLC over the now small river. C) photo of the marker at the base of one of the monuments taken in 2017 with a cm scale. The lower section shows ~6 cm of tidalites deposited over 4 monsoon seasons. Above are 4–6 cm of muddy deposits in the 2 years since the March 2015 dredging. (For interpretation of the references to colour in this figure legend, the reader is referred to the web version of this article.)

downward motion during the summer is due to loading by seasonal flooding and recharge of groundwater during the monsoon. It represents lithospheric-scale elastic deformation from an average of ~100×10^9 t (maximum ~150×10^9 t) of water, approximately 7.5% of the annual flow of the Ganges, Brahmaputra and Meghna Rivers that is sequestered in Bangladesh. As a result, continuous GNSS sites are necessary for accurate vertical rates. In Bangladesh, most antennas have been mounted on either stainless steel threaded rods cemented or epoxied into reinforced concrete buildings, or on tripods constructed out of welded stainless-steel rods driven into the ground. These systems capture subsidence where they are coupled to the ground, either the foundation of the building or at the ~2 m depth of the rods. Thus, GNSS, particularly building sites, may not measure the shallowest component of land surface subsidence (Keogh and Törnqvist, 2019).

We have processed all available GNSS data in the GBD using GAMIT/ GLOBK (Herring et al., 2018) with 16 International GNSS Service (IGS) stations used for stabilization. The vertical rates are given in Table S1 and the vertical time series for each of the sites is shown in Fig. S3. The first continuous GPS receivers in Bangladesh were installed in 2003 and the number of sites has grown over the years. We installed additional sites in southwest Bangladesh in 2012 and 2019, and rehabilitated older sites in 2014 and 2019. In this study, we have also included sites that have been installed by the Earth Observatory of Singapore (Mallick et al., 2019) and the continuous station deployed by the French IRD

(Institut de Recherche pour le Développement) through the Belmont Forum BanD-Aid project (Shum et al., 2014), which is maintained by CNRS-INSU (L'institut national des sciences de l'Univers). Continued measurements enhance the length of the record and thus the accuracy of subsidence rates. For all sites, the seasonal signal was removed by modeling the vertical deflection from water loading (Steckler et al., 2010). Water level was calculated using >300 daily river gauge and >1200 weekly ground water well measurements of the water table (Steckler et al., 2010; Nooner et al., in prep). The deflection from the regional water mass was calculated and removed using a best fit estimate of the Young's Modulus at each GNSS station with a best-fit trendline.

Fig. 8 shows results for the coastal zone of Bangladesh and India. The font size used is proportional to the square root of the times series length to reflect the reliability of the rate estimates. The rates for the newest sites, established in 2019, are still too short to be reliable and are not further considered. The larger symbols correspond to sites that have recorded data, sometimes intermittently, for 5–17 years. In the coastal belt, GNSS subsidence rates near the sandy Brahmaputra (Lower Meghna) river mouth are 4–5 mm/y (Fig. 8), similar to the Holocene rates determined by Grall et al. (2018) and lower than the river gauge sites (Becker et al., 2020). Farther west, we generally determined higher rates (5–8 mm/y for longer term stations) that exceed the Holocene average rates by several millimeters per year. We associate these higher

rates with muddier settings farther from the river mouth that may partially reflect additional near-surface consolidation and organic matter oxidation.

6. Discussion

6.1. Temporal and methodological controls on subsidence rates

The subsidence measurements presented here using different methodologies exhibit variations that show systematic patterns spatially—both in the horizontal and with depth—and temporally, (Fig. 10). In delta systems, it is recognized that thick sedimentary deposits loading the lithospheric plate enhance the subsidence rate. This isostatic adjustment to the sediment load likely contributes significantly to the long-term rate of subsidence (Karpytchev et al., 2018; Krien et al., 2019). Overall, subsidence rates are inversely time-dependent, with younger deposits consolidating at greater rates commensurate with their age (i.e., Sadler effect). We find this fundamental temporal control also holds true in the GBD. Holocene averaged subsidence rates (Grall et al., 2018) (Fig. 5) are lower than contemporary rates from tide gauges, GNSS, RSET and the vertical strainmeter. The rates from the 300–600 year old historic sites (Fig. 8; Sarker et al., 2012; Hanebuth et al., 2013; Chamberlain et al., 2020) are similar to the Holocene rates (Grall et al., 2018), providing a timescale for shallow sediment compaction similar to the Mississippi Delta (Jankowski et al., 2017; Keogh and Törnqvist, 2019). The Nile Delta also shows higher contemporary rates from GNSS and InSAR (6–10 mm/y; Gebremichael et al., 2018; Saleh and Becker, 2019) relative to Holocene rates (0–4.5 mm/y; Marriner et al., 2012).

GNSS subsidence rates from the past two decades (i.e., modern rates) generally show slightly higher values than the longer-term Holocene average rates (Figs. 5, 8). In the east, near the Lower Meghna River, rates are within a millimeter/year of the Holocene rates. However, farther west, GNSS subsidence rates are consistently a few mm/y higher than the longer-term rates. We tentatively ascribe this difference to greater

sediment compaction in the muddier sediments as described in the next section. The modern rates from tide and river gauges (Fig. 5; Becker et al., 2020) show an overall similarity to the GNSS rates in being slightly higher than the Holocene average values. However, the rates to the west are lower while the rates farther east are higher, inconsistent with attributing the GNSS rate differences to lithology.

Farther east, the river gauges show substantial subsidence (5.2 mm/ y) along and east of the Meghna River where the Holocene rates rapidly taper to zero (Fig. 5). We interpret this to reflect short-term subsidence associated with ongoing deformation above the locked subduction megathrust (Steckler et al., 2016; Mallick et al., 2019; Fig. 1), which may reach 3–4 mm/y (Oryan et al., 2020). Megathrust earthquakes would likely uplift this region. The 1762 M8.5 earthquake farther south along the Arakan coast resulted in 2–7 m of coastal uplift (Aung et al., 2008; Wang et al., 2013; Mondal et al., 2018). Over the longer term, we expect that the net effect of the current interseismic subsidence, and infrequent coseismic and postseismic uplift would be a slight net uplift related to shortening on the blind detachment folds in the frontal foldbelt (Betka et al., 2018; Mondal et al., 2018; Mallick et al., 2021). Thus, we interpret the difference between the shorter-term and longer-term rates to reflect the seismic cycle in this region.

The highest rates of subsidence are located north of the coastal zone near Dhaka (Figs. 5, 8) due to groundwater extraction. At Dhaka, there is a significant cone of withdrawal from water pumping such that the water table is currently >70 m below sea level and had been dropping by ~3 m/y since the 1980s (Akhter et al., 2009; Shamsudduha et al., 2009, 2011). GNSS sites at the center of the cone show subsidence rates of 9–13 mm/y (Fig. 8). The river gauges, covering a large area from the center of the cone out beyond the cone edge, yield 7.2 mm/y.

The devices measuring shallow subsidence, the RSET-MH and KHLC, show higher rates of 9–10 mm/y (Fig. 8). These instruments, located in sites of active sedimentation, include shallow subsidence not recorded by either the river gauges or GNSS. The anchor depth of the river gauges in Bangladesh is unknown; they average 20 m in the Mississippi Delta
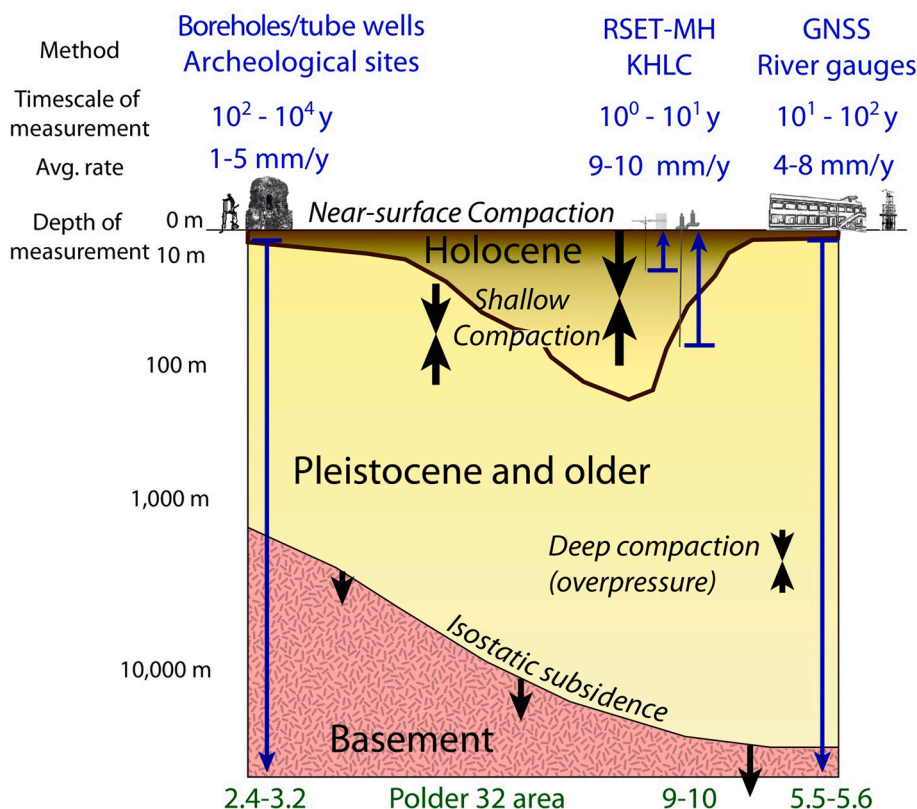

Fig. 10. Summary cartoon of subsidence and compaction measurements for a section centered the Brahmaputra incised valley (Fig. 2). Compacting sediments are in shades of brown to yellow with brown indicating faster compaction. The methods applied to distinguish rates and their timescales and values are shown in blue. The RSET and KHLC measure compaction from their base to the surface (upward arrows), while the other system measure subsidence below their base (downward arrows). At the bottom, values for long-term subsidence, shallow compaction, and short-term subsidence for the area around Polder 32, where we have all these systems, are given. (For interpretation of the references to colour in this figure legend, the reader is referred to the web version of this article.)

(Keogh and Törnqvist, 2019). The GNSS sites in Bangladesh are mainly installed on reinforced concrete buildings. The depth of pilings for the foundations are unknown, however, the ground is compacted before construction and there is no young sedimentation. Thus, shallow subsidence above some significant depth is not measured by either river gauges or GNSS. RSET-MH in the Mississippi Delta (Jankowski et al., 2017) show that shallow subsidence is primarily focused in the upper 5–10 m of sediment, averaging 6.4 ± 5.4 mm/year (Jankowski et al., 2017). GNSS-IR (interferometric reflectometry; Karegar et al., 2020) measures subsidence of the ground surface relative to anchored GNSS and found rates of 3–6 mm/y. Our results suggest similar amounts of shallow subsidence recorded by the RSET-MH and KHLC that are missed by the river gauges and GNSS sites because this subsidence occurs shallower than the depth at which the instruments are rooted. The GNSS do include deep subsidence that occurs below the base of the RSET or strainmeters. Thus, the total subsidence at a site with active sedimentation may be equal to the sum of the GNSS on buildings plus 3–6 mm/y of shallow subsidence, or equal to the RSET and KHLC with the addition of 2–3 mm/y or more of deep subsidence. The total subsidence may therefore reach values of 12–14 mm/y.

6.2. The role of lithology with subsidence

Differences in subsidence rates indicate that there is a considerable amount of ongoing shallow subsidence in the GBD due to sediment compaction, consolidation and organic matter degradation. GNSS subsidence rates are consistently a few mm/y higher than the longer-term rates in southwestern Bangladesh farther from the sandy main mouths of the Ganges River: the Hooghly River in India prior to the mid 1600s, the Arial Khan/Tetulia Channel from then until the mid 1900s and the Lower Meghna River since then (Fig. 1). Thus, the recent sediments are expected to be muddier in this region between the major rivers. Thicker total Holocene sediments upstream of the Swatch of No Ground canyon in SW Bangladesh (Fig. 1) may also play a role in contributing to subsidence from compaction here.

More local lithologic differences may also contribute to variations in compaction. For example, while the GNSS on Polder 32 measures 5.6 mm/y subsidence, the RSET-MHs 6–9 km away in the Sundarbans record 9.7 mm/y of shallow subsidence (Figs. 8, 10). RSET-MH subsidence values only include compaction above the base of the rods (in this case, 24.4 m). Meanwhile, KHLC to the NE shows the shallow subsidence is distributed over a greater depth range (Fig. 9). While the total compaction of 9 mm/y is similar between KHLC and the RSET-MH, KHLC only records 3.1 and 5.6 mm/y at the shallowest 20 and 40 m depth wells. This indicates significant variability in the shallow subsidence between sites, with the natural Sundarbans mangrove forest having more compaction occurring at very shallow depths (Bomer et al., 2020). This may be due to the muddier nature of the deposits in the Sundarbans and the greater root density in the mangroves (Bomer et al., 2020) since muddy sediments undergo more shallow compaction than sands (Kominz et al., 2011). At the compaction meter site, in contrast, the deposits beneath the recent channel fill were mainly very fine sand (Wilson et al., 2017; Chamberlain et al., 2020). Furthermore, shallow subsidence in natural areas such as the Sundarbans mangrove forest is driven by seasonal dewatering of the shallow subsurface (<2 m) with lowering of the groundwater table during the dry season (Bomer et al., 2020).

7. Synthesis and implications

The combination of multiple methods of estimating subsidence and compaction in the GBD leads to a pattern of subsidence varying with timescale, spatial location and depth (Fig. 10). Subsidence is lower at longer timescales. We attribute this to the rate at which fresh young sediments are undergoing initial compaction and organic matter degradation. As the rates for multi-century historic sites and Holocene

sites are similar, we conclude this occurs at the century time scale and the longer time scales reflect compaction and isostasy from a more stable sediment porosity profile. Grall et al. (2018) found that the longer-term rates increase from near zero at the Hinge Zone to 4.5 mm/y near the coast. This likely reflects the increase in both the Holocene and total sediment thickness, as well as the increasing proportion of mud from the Hinge Zone toward the coast. River gauges and GNSS systems yield rates that are a few millimeters a year higher than the long-term rates (Fig. 10). These systems are rooted in the ground or on buildings and therefore do not measure very near surface compaction (<5 m). However, ongoing compaction of their underlying sediments contributes to greater current rates of subsidence than the long-term rates.

Systems that measure shallow subsurface compaction and subsidence (<100 m), such as RSET-MH and optical fiber strain meters, yield considerably higher rates of 9–10 mm/y (Fig. 10). Neither of these systems measure deeper subsidence, so the total subsidence rate must be at least a few millimeters a year higher. These results also indicate that there is considerable subsidence arising from near-surface processes related to compaction, sediment consolidation and organic matter degradation. The upper few meters of sediments tend to be finer grained (Wilson and Goodbred, 2015; Bomer et al., 2020). These sediments are reworked by shifting channels so that the preserved sediments are generally coarse, although channels are less mobile in the tidal realm. However, these loose ephemeral sediments may contribute to high compaction rates in the near surface that could reach 5 mm/y or more. We note the depth distribution of the overall compaction contribution remains uncertain. The KHLC compaction meter suggests most compaction in the southwest region is occurring in the Holocene sediment deposited within the incised valleys. However, the RSET-MH suggests that most of the compaction may be even shallower, and that groundwater hydrology may play a large role. This significant shallow contribution needs further investigation to better quantify it.

Deep compaction of sediments below the Holocene appears to be limited, and we find that the bulk of the subsidence from compaction is from within Holocene-aged sediments. Viscoelastic modeling (Karpytchev et al., 2018; Krien et al., 2019) suggest 1–3 mm/y of isostatic adjustment from the sediment load. As noted earlier, the pre-Holocene sediments below the Brahmaputra incised valley may be overcompacted and contribute little to current rates. At depths greater than 3–5 km, the sediments in the GBD are highly overpressured (Zahid and Uddin, 2005), which also means that dewatering and compaction of these sediments are limited (Gordon and Flemings, 1998).

Given spatial and temporal variability of subsidence rates revealed here, we must ask which rates are significant for people living on a delta? When planning adaptations to rising sea level in the GBD, the physical environment and nature of any construction must be seriously considered. Specifically, it should be acknowledged that subsidence rates can differ, even locally, and this has implications for nature-based solutions and/or hard constructed solutions. For example, designs for embankment construction must take rates of sea level rise and ground subsidence into account. Reinforced concrete buildings, such as those hosting the GNSS, are subsiding at 4–8 mm/y. Are the embankments constructed of compacted sand and pilings faced with concrete blocks settling at a rate similar to the GNSS? In contrast, in regions of active sedimentation, we find significantly higher rates of subsidence. Is this high rate due to very near surface consolidation only present where there is active sedimentation? If sedimentation stops, how long will higher subsidence rates continue? From the historic sites, we estimate it is likely shorter than 300–600 years. Still, the findings suggest that natural subsidence processes can continue for decades to centuries.

At Polder 32, we have all the different types of measurements available in a limited area. We found 2.4–3.2 mm/y of long-term subsidence, increasing to 5.5–5.6 mm/y of short-term subsidence (Fig. 10, bottom). Shallow compaction measured nearby reaches 9–10 mm/y. Within Polder 32, Auerbach et al. (2015) found that there was a loss of 1.0–1.5 m of elevation relative to the Sundarbans over 50 years since the

embankment was built. Using their values of 11 mm/y of sediment accretion in the Sundarbans and an extra 20 cm of elevation loss from root extraction, these findings suggest 5–15 mm/y of subsidence in the polder interior since the embankment precluded natural sedimentation. This suite of values is consistent with the 3–6 mm/y of very shallow compaction seen in the Mississippi Delta (Jankowski et al., 2017; Karegar et al., 2020). This means that for restoring polder elevation through nature-based solutions, such as Tidal River Management (Shampa and Pramanik, 2012; Islam et al., 2021), sediment volumes that are required need to account for expected compaction which will occur in the shallow subsurface and the resultant relatively high subsidence rate.

These results illustrate the complexity of subsidence and compaction as a function of depth, space and time, and begins to unravel the values in a densely-populated, vulnerable delta. One cannot characterize subsidence with a single value without reference to its context. While further work is still required to better understand the variability of subsidence rates and their relationship to the underlying geology and the physical processes that contribute to subsidence, our results begin to provide values for the Ganges-Brahmaputra Delta. Similar relative rates likely apply to other deltas as well. Which values are appropriate for mitigation of sea level rise and maintenance of the GBD and other deltas depend on both the local and regional settings. For instance, locally, subsidence appears to be lower for embankments and buildings, but higher for sites of active sedimentation. All of these rates can be exacerbated by anthropogenic modification, such as fluid withdrawal.

Author contributions

MSS: Wrote text, drafted figures, interpreted results, installed GNSS and helped with other equipment.

BO: Processed GNSS data, wrote and edited text, drafted figure.

CAW: Installed and analyzed RSETs, wrote and edited text.

CG: Analyzed well data, wrote and edited text.

SLN: Helped install GNSS and compaction meter, seasonal correction to GNSS data, edited text.

DRM: Tide gauge analysis, aided in GNSS processing, augering at Temple.

SHA: Installation and maintenance of GNSS.

SD: Installation of compaction meter and analysis of results.

SLG: Analysis of tube well data, augering at Temple.

Declaration of Competing Interest

The authors have no competing interests.

Acknowledgements

Appendix A. Supplementary data

Supplementary data to this article can be found online at https://doi.org/10.1016/j.earscirev.2021.103887.

References

Akhter, H., Ahmed, M.S., Rasheed, K.B.S., 2009. Spatial and temporal analysis of groundwater level fluctuations in Dhaka City, Bangladesh, Asian. J. Earth Sci. 2, 49–57.

Akhter, S.H., 2010. Earthquakes of Dhaka. In: Islam, M.A. (Ed.), Environment of Capital Dhaka—Plants Wildlife Gardens Parks Air Water and Earthquake. Asiatic Society of Bangladesh, Bangladesh, pp. 401–426.

Alam, M., 1996. Subsidence of the Ganges–Brahmaputra delta of Bangladesh and associated drainage, sedimentation and salinity problems. In: Milliman, J.D., Haq, B.U. (Eds.), Sea-Level Rise and Coastal Subsidence. Kluwer Academic Publishers, Dordrecht, pp. 169–192.

Alauddin, M., Hamid, M.A., 1999. In: Smith, P.T. (Ed.), Shrimp Culture in Bangladesh with Emphasis on Social and Economic Aspects. Towards Sustainable Shrimp Culture in Thailand and the Region. Australian Centre for International Agricultural Research, Canberra, pp. 53–62.

Allison, M.A., 1998. Historical changes in the Ganges-Brahmaputra Delta front. J. Coast. Res. 14 (4), 1269–1275.

Allison, M.A., Khan, S.R., Goodbred, S.L., Kuehl, S.A., 2003. Stratigraphic evolution of the late Holocene Ganges-Brahmaputra lower delta plain. Sediment. Geol. 155 (3), 317–342. https://doi.org/10.1016/S0037-0738(02)00185-9.

van Asselen, S., 2011. The contribution of peat compaction to total basin subsidence: Implications for the provision of accommodation space in organic-rich deltas. Basin Res. 23, 239–255.

van Asselen, S., Erkens, G., Stouthamer, E., Woolderink, H., Geeraert, R., Hefting, M.M., 2018. The relative contribution of peat compaction and oxidation to subsidence in built-up areas in the Rhine-Meuse delta, the Netherlands. Sci. Total Environ. 636, 177–191. https://doi.org/10.1016/j.scitotenv.2018.04.141.

Athy, L.F., 1930. Density, porosity, and compaction of sedimentary rocks. Bull. Am. Ass. Petrol. Geol. 14, 1–24.

Auerbach, L., Goodbred, S., Mondal, D., Wilson, C., Ahmed, K.R., Roy, K., Steckler, M., Gilligan, J., Ackerly, B., 2015. In the balance: natural v. Embanked landscapes in the Ganges-Brahmaputra Tidal Delta Plain. Nat. Clim. Chang. 5, 153–157. https://doi.org/10.1038/nclimate2472.

Aung, T.T., Satake, K., Okamura, Y., Shishikura, M., Swe, W., Saw, H., Swe, T.L., Tun, S.T., Aung, T., 2008. Geologic evidence for three great earthquakes in the past 3400 years off Myanmar. J. Earthq. Tsunami 2, 259–265.

Bahr, D.B., Hutton, E.W.H., Syvitski, J.P.M., Pratson, L.F., 2001. Exponential approximations to compacted sediment porosity profiles. Computers & Geosciences 27, 691–700.

Becker, M., Papa, F., Karpytchev, M., Delebecque, C., Krien, Y., Khan, J.U., Ballu, V., Durand, F., Le Cozannet, G., Islam, A.K.M.S., Calmant, S., Shum, C.K., 2020. Water level changes, subsidence, and sea level rise in the Ganges–Brahmaputra–Meghna delta. Proc. Natl. Acad. Sci. 117 (4), 1867–1876. https://doi.org/10.1073/pnas.1912921117.

Betka, P.M., Seeber, L., Thomson, S., Steckler, M.S., Sincavage, R., Zoramthara, C., 2018. Slip partitioning above a shallow, weak décollement beneath the Indo-Burman accretionary prism. Earth Planet. Sci. Lett. 503, 17–28. https://doi.org/10.1016/j.epsl.2018.09.003.

Best, J.L., Ashworth, P.J., Sarker, M.H., Roden, J.E., 2007. The Brahmaputra-Jamuna River. In: Gupta, A. (Ed.), Bangladesh. In Large Rivers: Geomorphology and Management, pp. 395–433.

Blewitt, G., Lavallée, D., 2002. Effect of annual signals on geodetic velocity. J. Geophys. Res. 107, 2145–2156. https://doi.org/10.1029/2001JB000570.

Blum, M.D., Roberts, H.H., 2009. Drowning of the Mississippi Delta due to insufficient sediment supply and global sea-level rise. Nat. Geosci. 2, 488–491. https://doi.org/10.1038/NGEO553.

Bomer, E.J., Wilson, C.A., Hale, R.P., Hossain, A.N.M., Rahman, F.M.A., 2020. Surface elevation and sedimentation dynamics in the Ganges-Brahmaputra tidal delta plain, Bangladesh: implications for the sustainability of natural and human-impacted coastal systems. Catena. 187, 104312.

Brammer, H., 1990. Floods in Bangladesh: Geographical background to the 1987 and 1988 floods. Geogr. J. 156, 12–22. https://doi.org/10.2307/635431.

Brammer, H., 2014. Bangladesh's dynamic coastal regions and sea-level rise. Clim. Risk Manag. 1, 51–62.

Brown, S., Nicholls, R.J., 2015. Subsidence and human influences in mega deltas: the case of the Ganges-Brahmaputra-Meghna. Sci. Total Environ. 527–528, 362–374.

Cahoon, D.R., Reed, D.J., Day, J.W., 1995. Estimating shallow subsidence in microtidal salt marshes of the southeastern United States: Kaye and Barghoorn revisited. Mar. Geol. 128, 1–9. https://doi.org/10.1016/0025-3227(95)00087-F.

Cahoon, D.R., Lynch, J.C., Perez, B.C., Segura, B., Holland, R.D., Stelly, C., et al., 2002. High precision measurements of wetland sediment elevation: II. The rod surface elevation table. J. Sediment. Res. 72, 734–739. https://doi.org/10.1306/020702720734.

Chamberlain, E.L., Wallinga, J., Reimann, T., Goodbred, S.L., Steckler, M., Shen, Z., Sincavage, R., 2017. Luminescence dating of delta sediments: novel approaches explored for the Ganges-Brahmaputra- Meghna delta. Quat. Geochronol. 41, 97–111. https://doi.org/10.1016/j.quageo.2017.06.006.

Chamberlain, E.L., Goodbred, S.L., Hale, R., Steckler, M.S., Wallinga, J., Wilson, C., 2020. Integrating geochronologic and instrumental approaches across the Bengal Basin. Earth Surf. Process. Landf. 45, 56–74. https://doi.org/10.1002/esp.4687.

Chapman, R.E., 1983. Chapter 3: Compaction of sediment and sedimentary rocks, and its consequences. In: Chapman, R.E. (Ed.), Petroleum Geology, Developments in Petroleum Science 16. Elsevier, Amsterdam, pp. 41–65.

DeWolf, S., Nooner, S.L., Steckler, M.S., Zumberge, M.A., Akhter, S.H., 2013. Optical Fiber Borehole Strainmeter Arrays for Measuring Sediment Compaction in

Bangladesh, Abstract EP31A-0831 presented at 2013 Fall Meeting, AGU, San Francisco, Calif., 9–13 Dec.

Dixon, T.H., Amelung, F., Ferretti, A., Novali, F., Rocca, F., Dokka, R., et al., 2006. Space geodesy: subsidence and flooding in New Orleans. Nature 441 (7093), 587–588. https://doi.org/10.1038/441587a.

Dunn, F.E., Darby, S.E., Nicholls, R.J., Cohen, S., Zarfl, C., Fekete, B.M., 2019. Projections of declining fluvial sediment delivery to major deltas worldwide in response to climate change and anthropogenic stress. Environ. Res. Lett. 14, 084034 https://doi.org/10.1088/1748-9326/ab304e.

Eaton, Richard M., 1993. The Rise of Islam and the Bengal Frontier, 1204–1760. University of California Press, Berkeley, 192pp.

Edmonds, D.A., Caldwell, R.L., Brondizio, E.S., Siani, S.M.O., 2020. Coastal flooding will disproportionately impact people on river deltas. Nat. Commun. 11, 474. https://doi.org/10.1038/s41467-020-18531-4.

Ericson, J.P., Vörösmarty, C.J., Dingman, S.L., Ward, L.G., Meybeck, M., 2006. Effective Sea-level rise and deltas: causes of change and human dimension implications. Glob. Planet. Chang. 50, 63–82. https://doi.org/10.1016/j.gloplacha.2005.07.004.

Erkens, G., van der Meulen, M.J., Middelkoop, H., 2016. Double trouble: subsidence and CO2 respiration due to 1,000 years of Dutch coastal peatlands cultivation. Hydrogeol. J. 24, 551–568. https://doi.org/10.1007/s10040-016-1380-4.

Gebremichael, E., Sultan, M., Becker, R., El Bastawesy, M., Cherif, O., Emil, M., 2018. Assessing land deformation and sea encroachment in the Nile Delta: a radar interferometric and inundation modeling approach. J. Geophys. Res. Solid Earth 123, 3208–3224. https://doi.org/10.1002/2017JB015084.

Giosan, L., Syvitski, J., Constantinescu, S., Day, J., 2014. Protect the world's deltas. Nature 516, 31–33.

Gluyas, J., Cade, C.A., Kupecz, J.A., Gluyas, J., Bloch, S., 1997. Prediction of Porosity in Compacted Sands, AAPG Memoir 69: Reservoir Quality Prediction in Sandstones and Carbonates, pp. 19–27.

Goodbred, S.L., Kuehl, S.A., Steckler, M., Sarker, M.H., 2003. Controls on facies distribution and stratigraphic preservation in the Ganges-Brahmaputra delta sequence. Sediment. Geol. 155, 301–316.

Goodbred, S.L., Paolo, P.M., Ullah, M.S., Pate, R.D., Khan, S.R., Kuehl, S.A., Singh, S.K., Rahaman, W., 2014. Piecing together the Ganges-Brahmaputra-Meghna River delta: use of sediment provenance to reconstruct the history and interaction of multiple fluvial systems during Holocene delta evolution. GSA Bull. 126, 1495–1510. https://doi.org/10.1130/B30965.1.

Gordon, D.S., Flemings, P.B., 1998. Generation of overpressure and compaction-driven fluid flow in a Plio-Pleistocene growth-faulted basin, Eugene Island 330, offshore Louisiana. Basin Res. 10, 177–196.

Goswami, D.C., 1985. Brahmaputra River, Assam, India: basin denudation and channel aggradation. Water Resources Research 21, 959–978.

Grall, C., Steckler, M.S., Pickering, J.L., Goodbred, S., Sincavage, R., Paola, C., Akhter, S.H., Spiess, V., 2018. A base-level stratigraphic approach to determining Holocene subsidence of the Ganges–Meghna–Brahmaputra Delta plain. Earth Planet. Sci. Lett. 499, 23–36. https://doi.org/10.1016/j.epsl.2018.07.008.

Grimaud, J.-L., Grall, C., Goodbred, S., Steckler, M.S., Sincavage, R., Pickering, J.L., Paola, C., Seeber, L., Hossain, M.S., 2020. Flexural deformation controls on late Quaternary sediment dispersal in the Garo-Rajmahal Gap, NW Bengal Basin. Basin Res. 32, 1242–1260. https://doi.org/10.1111/bre.12425.

Hanebuth, T.J.J., Kudrass, H.R., Linstaedter, J., Islam, B., Zander, A.M., 2013. Rapid coastal subsidence in the central Ganges–Brahmaputra Delta (Bangladesh) since the 17th century deduced from submerged salt-producing kilns. Geology 41 (9), 987–990. https://doi.org/10.1130/G34646.1.

Hedberg, H.D., 1936. Gravitational compaction of clays and shales. Am. J. Sci. 31, 241–287.

Herring, T.A., King, R.W., Floyd, M.A., McClusky, S.C., 2018. Introduction to GAMIT/GLOBK Release, 10.7, 54p.

Higgins, S.A., Overeem, I., Steckler, M.S., Syvitski, J.P.M., Seeber, L., Akhter, S.H., 2014. InSAR measurements of compaction and subsidence in the Ganges–Brahmaputra Delta, Bangladesh. J. Geophys. Res. Earth Surf. 119 (8) https://doi.org/10.1002/2014JF003117 (2014JF003117).

Hoque, M., Alam, M., 1997. Subsidence in the lower deltaic areas of Bangladesh. Mar. Geod. 20 (1), 105–120. https://doi.org/10.1080/01490419709388098.

Islam, Md.F., Middelkoop, H., Schot, P.P., Dekker, S.C., Griffioen, J., 2021. Spatial and seasonal variability of sediment accumulation potential through controlled flooding of the beels located in the polders of the Ganges-Brahmaputra-Meghna delta of Southwest Bangladesh. Hydrol. Process. 35, 14119. https://doi.org/10.1002/hyp.14119.

Ismaiel, M., Krishna, K.S., Srinivas, K., Mishra, J., Saha, D., 2019. Crustal architecture and Moho topography beneath the eastern Indian and Bangladesh margins – new insights on rift evolution and the continent–ocean boundary. J. Geo. Soc. 176, 553–573. https://doi.org/10.1144/jgs2018-131.

Jankowski, K.L., Törnqvist, T.E., Fernandes, A.M., 2017. Vulnerability of Louisiana's coastal wetlands to present-day rates of relative sea-level rise. Nat. Commun. 8, 14792. https://doi.org/10.1038/ncomms14792.

Karegar, M.A., Larson, K.M., Kusche, J., Dixon, T.H., 2020. Novel quantification of shallow sediment compaction by GPS interferometric reflectometry and implications for flood susceptibility. Geophys. Res. Lett. 47 https://doi.org/10.1029/2020GL087807 e2020GL087807.

Karpytchev, M., Ballu, V., Krien, Y., Becker, M., Goodbred, S., Spada, G., Calmant, S., Shum, C.K., Khan, Z., 2018. Contributions of a strengthened early Holocene monsoon and sediment loading to present-day subsidence of the Ganges-Brahmaputra Delta. Geophys. Res. Lett. 45, 1433–1442. https://doi.org/10.1002/2017GL076388.

Keogh, M.E., Törnqvist, T.E., 2019. Measuring rates of present-day relative sea-level rise in low-elevation coastal zones: a critical evaluation. Ocean Sci. 15, 61–73. https://doi.org/10.5194/os-15-61-2019.

Kominz, M.A., Patterson, K., Odette, D., 2011. Lithology dependence of porosity in slope and deep marine sediments. J. Sediment. Res. 2011 (81), 730–742. https://doi.org/10.2110/jsr.2011.60.

Kondolf, G.M., Rubin, Z.K., Minear, J.T., 2014. Dams on the Mekong: cumulative sediment starvation. Water Resour. Res. 50, 5158–5169.

Kooi, H., DeVries, J.J., 1998. Land subsidence and hydrodynamic compaction of sedimentary basins. Hydrology and Earth System Sciences 2, 159–171.

Krien, Y., Karpytchev, M., Ballu, V., Becker, M., Grall, C., Goodbred, S., Calmant, S., Shum, C.K., Khan, Z., 2019. Present-day subsidence in the Ganges-Brahmaputra-Meghna delta: Eastern amplification of the Holocene sediment loading contribution. Geophys. Res. Lett. 49, 10764–10772.

Mallick, R., Lindsey, E.O., Feng, L., Hubbard, J., Banerjee, P., Hill, E.M., 2019. Active convergence of the India-Burma-Sunda plates revealed by a new continuous GPS network. J. Geophys. Res. Solid Earth 124. https://doi.org/10.1029/2018JB016480.

Mallick, R., Bürgmann, R., Johnson, K., Hubbard, J., 2021. A unified framework for earthquake sequences and the growth of geological structure in fold-thrust belts. J. Geophys. Res. Solid Earth 126. https://doi.org/10.1029/2021JB022045 e2021JB022045.

Meckel, T.A., ten Brink, U.S., Williams, S.J., 2007. Sediment compaction rates and subsidence in deltaic plains: numerical constraints and stratigraphic influences. Basin Res 19, 19–31.

Marriner, N., Flaux, C., Morhange, C., Kaniewski, D., 2012. Nile Delta's sinking past: Quantifiable links with Holocene compaction and climate-driven changes in sediment supply? Geology 40 (12), 1083–1086. https://doi.org/10.1130/G33209.1.

Milliman, J.D., Farnsworth, K.L., 2011. River Discharge to the Coastal Ocean: A Global Synthesis. Cambridge University Press, 384 pp.

Milliman, J.D., Broadus, J.M., Gable, F., 1989. Environmental and economic implications of rising Sea Level and Subsiding Deltas: the Nile and Bengal examples. Ambio 18, 340–345.

Minderhoud, P.S.J., Erkens, G., Pham, V.H., Bui, V.T., Erban, L., Kooi, H., Stouthamer, E., 2017. Impacts of 25 years of groundwater extraction on subsidence in the Mekong delta, Vietnam. Environ. Res. Lett. 12, 064006 https://doi.org/10.1088/1748-9326/aa7146.

Mirza, M.M.Q., 2003. Three recent extreme floods in Bangladesh: a hydro-meteorological analysis. Nat. Hazards 28, 35–64.

Mitra, S., Priestley, K.F., Borah, K., Gaur, V.K., 2018. Crustal structure and evolution of the Eastern Himalayan plate boundary system, Northeast India. J. Geophys. Res. Solid Earth 123, 621–640. https://doi.org/10.1002/2017JB014714.

Mondal, D., McHugh, C.M., Mortlock, R.M., Steckler, M.S., Mustaque, S., 2018. Microatolls document the 1762 and prior earthquakes along the southeast coast of Bangladesh. Tectonophysics 745, 196–213. https://doi.org/10.1016/j.tecto.2018.07.020.

Nienhuis, J.H., Ashton, A.D., Edmonds, D.A., Hoitink, A.J.F., Kettner, A.J., Rowland, J.C., Törnqvist, T.E., 2020. Global-scale human impact on delta morphology has led to net land area gain. Nature 577, 514–518. https://doi.org/10.1038/s41586-019-1905-9.

Oryan, B., Steckler, M.S., Mondal, D.R., Akhter, S.H., Singha, S., Grall, C., Lindsey, E.O., 2020. The Indo-Burma Detachment Geometry Constrained by an Updated Vertical and Horizontal GPS Velocity Field in Bangladesh, Abstract T048-0021, AGU Fall Meeting, Dec. 1-17, 2020.

Ostanciaux, É., Husson, L., Choblet, G., Robin, C., Pedoja, K., 2012. Present-day trends of vertical ground motions along the coast lines. Earth Sci. Rev. 110, 74–92. https://doi.org/10.1016/j.earscirev.2011.10.004.

Palamenghi, L., 2012. Tectonic and Sea Level Control on the Transport and Depositional Processes in a Siliciclastic Sedimentary Basin. Insights from the Ganges-Brahmaputra Delta, Bengal Basin, Bangladesh (Ph.D. Thesis). University of Bremen, 166pp.

Parua, P.K., 2010. The Ganga: Water Use in the Indian Subcontinent. Water Science and Technology Library, Vol. 64. Springer. https://doi.org/10.1007/978-90-481-3103-7, 404 pp.

Paszkowski, A., Goodbred, S., Borgomeo, E., Khan, M.S.A., Hall, J.W., 2021. Geomorphic change in the Ganges–Brahmaputra–Meghna delta. Nat. Rev. Earth Environ. 2, 763–780. https://doi.org/10.1038/s43017-021-00213-4.

Pawlowicz, R., Beardsley, B., Lentz, S., 2002. Classical tidal harmonic analysis including error estimates in MATLAB using T_TIDE. Comput. Geosci. 28, 929–937.

Pethick, J., Orford, J.D., 2013. Rapid rise in effective sea-level in Southwest Bangladesh: its causes and contemporary rates. Glob. Planet. Chang. 111, 237–245. https://doi.org/10.1016/j.gloplacha.2013.09.019.

Pickering, J.L., Goodbred Jr., S.L., Reitz, M.D., Hartzog, T.R., Mondal, D.R., Hossain, M.S., 2014. Late Quaternary sedimentary record and Holocene channel avulsions of the Jamuna and Old Brahmaputra River valleys in the upper Bengal delta plain. Geomorphology 227, 123–136. https://doi.org/10.1016/j.geomorph.2013.09.021.

Reitz, M.D., Pickering, J.L., Goodbred, S.L., Paola, C., Steckler, M.S., Seeber, L., Akhter, S.H., 2015. Effects of tectonic deformation and sea level on river path selection: theory and application to the Ganges–Brahmaputra–Meghna River Delta. J. Geophys. Res. Earth Surf. https://doi.org/10.1002/2014JF003202.

Rogers, K., Overeem, I., 2017. Doomed to drown? Sediment dynamics in the human-controlled floodplains of the active Bengal Delta. Elem. Sci. Anthropocene 5, 66. https://doi.org/10.1525/elementa.250.

Rogers, K.G., Goodbred, S.L., Mondal, D.R., 2013. Monsoon sedimentation on the 'abandoned' tide-influenced Ganges-Brahmaputra delta plain. Estuar. Coast. Shelf Sci. 131, 297–309. https://doi.org/10.1016/j.ecss.2013.07.014.

Sadler, P.M., 1981. Sediment accumulation rates and the completeness of stratigraphic sections. J. Geol. 89, 569–584.

Saleh, M., Becker, M., 2019. New estimation of Nile Delta subsidence rates from InSAR and GPS analysis. Environ. Earth Sci. 78 https://doi.org/10.1007/s12665-018-8001-6.

Sarker, M.H., Thorne, C.R., 2006. Morphological response of the Brahmaputra-Padma-lower Meghna river system to the Assam earthquake of 1950. In: Smith, G.H.S., Best, J.L., Bristow, C.S., Petts, G.E. (Eds.), Braided Rivers: Process, Deposits, Ecology and Management. Special Publication 36 of the IAS, Blackwell Publishing, UK, pp. 289–310.

Sarker, M.H., Choudhury, G.A., Akter, J., Hore, S.K., 2012. Bengal Delta Not Sinking at a Very High Rate. Daily Star (23rd December 2012).

Sarker, M.H., Akter, J., Rahman, Md.M., 2013. Century-scale dynamics of the Bengal Delta and future development, 4th International Conference on Water & Flood Management (ICWFM-2013), 91–104.

Sarma, J.N., 2005. Fluvial process and morphology of the Brahmaputra River in Assam, India. Geomorphology 70, 226–256.

Sclater, J.G., Christie, P.A., 1980. Continental stretching; An explanation of the post Mid-Cretaceous subsidence of the central North Sea basin. J. Geophys. Res. 85, 3711–3739.

Shampa, M., Pramanik, I.M., 2012. Tidal River Management (TRM) for selected Coastal Area of Bangladesh to Mitigate Drainage Congestion. Int. J. Sci. Technol. Res. 1, 1–6.

Shamsudduha, M., Chandler, R.E., Taylor, R.G., Ahmed, K.M., 2009. Recent trends in groundwater levels in a highly seasonal hydrological system: the Ganges-Brahmaputra-Meghna Delta. Hydrol. Earth Syst. Sci. 13, 2373–2385.

Shamsudduha, M., Taylor, R.G., Ahmed, K.M., Zahid, A., 2011. The impact of intensive groundwater abstraction on recharge to a shallow regional aquifer system: evidence from Bangladesh. Hydrogeology Journal 19, 901–916.

Sharma, S., Deshpande, S., 2017. Architectural strategies used in Hindu temples to emphasize sacredness. J. Architect. Plann. Res. 34 (4), 309–319.

Sheldon, N.D., Retallack, G.J., 2001. Equation for compaction of paleosols due to burial. Geology 29, 247–250.

Shum, C., Liibusk, A., Ahmed, R., Braun, B., Ballu, V., Calmant, S., Chen, J., Guo, J., Hossain, F., Hossain, M., Jenkins, C., Khan, Z., Kuhn, M., Kusche, J., Papa, F., Becker, M., Bernzen, A., Brachet, C., Calzas, M., Dai, C., Francis, O., Jia, Y., Kim, J., Kuo, C., Maillard, D., Mayet, C., Rietbroek, R., Shang, K., Testut, L., Tseng, K., Uebbing, B., Valty, P., Wan, J., Zhu, K., 2014. Quantifying and Projecting Relative Sea-Level Rise at the Regional Scale: The Bangladesh Sea-Level Project (BanD-AID), Abstract G21B-0439, EOS Trans., Fall American Geophysical Union Meeting, San Francisco, December 15–19.

Sincavage, R., Goodbred, S., Pickering, J., 2017. Holocene Brahmaputra River path selection and variable sediment bypass as indicators of fluctuating hydrologic and climate conditions in Sylhet Basin, Bangladesh. Basin Res. 30 (302–320), 2017. https://doi.org/10.1111/bre.12254.

Singh, A., Bhushan, K., Singh, C., Steckler, M.S., Akhter, S.H., Seeber, L., Kim, W.-Y., Tiwari, A.K., Biswas, R., 2016. Crustal structure and tectonics of Bangladesh: New constraints from inversion of receiver functions. Tectonophysics 680, 99–112. https://doi.org/10.1016/j.tecto.2016.04.046.

Slingerland, R., Smith, N.D., 2004. River Avulsions and their deposits. Annu. Rev. Earth Planet. Sci. 32, 255–283.

Steckler, M.S., Akhter, S.H., Seeber, L., 2008. Collision of the Ganges-Brahmaputra Delta with the Burma Arc: Implications for earthquake hazard. Earth Planet. Sci. Lett. 273, 367–378.

Steckler, M.S., Nooner, S.L., Akhter, S.H., Chowdhury, S.K., Bettadpur, S., Seeber, L., Kogan, M.G., 2010. Modeling Earth deformation from monsoonal flooding in Bangladesh using hydrographic, GPS, and Gravity Recovery and climate Experiment (GRACE) data. J. Geophys. Res. Solid Earth 115, B08407. https://doi.org/10.1029/2009JB007018.

Steckler, M.S., Mondal, D., Akhter, S.H., Seeber, L., Feng, L., Gale, J., Hill, E.M., Howe, M., 2016. Locked and loading megathrust linked to active subduction beneath the Indo-Burman Ranges. Nat. Geosci. 9, 615–618. https://doi.org/10.1038/ngeo2760.

Syvitski, J.P.M., Vörösmarty, C.J., Kettner, A.J., Green, P., 2005. Impact of humans on the flux of terrestrial sediment to the global coastal ocean. Science 308, 376–380. https://doi.org/10.1126/science.1109454.

Syvitski, J.P.M., Kettner, A.J., Overeem, I., Hutton, E.W.H., Hannon, M.T., Brakenridge, G.R., Day, J., Vörösmarty, C., Saito, Y., Giosan, L., Nicholls, R.J., 2009. Sinking deltas due to human activities. Nat. Geosci. 2, 681–686. https://doi.org/10.1038/ngeo629.

Terzaghi, K., Peck, R.B., 1967. Soil Mechanics in Engineering Practice, 2nd ed. Wiley, New York. 729pp.

Tessler, Z., Vörösmarty, C.J., Grossberg, M., Gladkova, I., Aizenman, H., Syvitski, J.P.M., Foufoula-Georgiou, E., 2015. Profiling risk and sustainability in coastal deltas of the world. Science 349 (6248), 638–643.

Tessler, Z.D., Vörösmarty, C.J., Overeem, I., Syvitski, J.P., 2018. A model of water and sediment balance as determinants of relative sea level rise in contemporary and future deltas. Geomorphology. 305, 209–220. https://doi.org/10.1016/j.geomorph.2017.09.040.

Wang, Y., Shyu, J.B.H., Sieh, K., Chiang, H.-W., Wang, C.-C., Aung, T., Lin, Y.N., Shen, C.-C., Min, S., Than, O., Lin, K.K., Tun, S.T., 2013. Permanent upper plate deformation in western Myanmar during the great 1762 earthquake: Implications for neotectonic behavior of the northern Sunda megathrust. J. Geophys. Res. Solid Earth 118, 1277–1303. https://doi.org/10.1002/jgrb.50121.

Wilson, C., Goodbred, S., Small, C., Gilligan, J., Sams, S., Mallick, B., Hale, R., 2017. Widespread infilling of tidal channels and navigable waterways in the human-modified tidal deltaplain of Southwest Bangladesh. Elem.-Sci. Anthropocene 5, 78. https://doi.org/10.1525/elementa.263.

Wilson, C., Bomer, J., Akter, S., Rana, M., Steckler, M., Oryan, B., 2021. Impacts of Poldering: Elevation Change, Sediment Dynamics, and Subsidence in the Natural and Human-altered Ganges Brahmaputra Tidal Deltaplain. Abstract EGU21–13928 Presented at EGU General Assembly 2021, April 19–30.

Wilson, C.A., Goodbred, S.L., 2015. Construction and Maintenance of the Ganges-Brahmaputra Delta: linking Process, Morphology, and Stratigraphy. Annu. Rev. Mar. Sci. 7, 67–88.

Woods, C., Overeem, I., Tiampo, K., Steckler, M., 2019. DInSAR Sentinel-1A time series analysis to map subsidence of the Ganges-Brahmaputra-Meghna Delta, Abstract G13B-0538 presented at AGU Fall Meeting, San Francisco, Dec 9-13, 2019.

Zahid, K.M., Uddin, A., 2005. Influence of overpressure on formation velocity evaluation of Neogene strata from the eastern Bengal Basin, Bangladesh. J. Asian Earth Sci. 25, 419–429.